AGU PUBLICATIONS

Geochemistry, Geophysics, Geosystems

RESEARCH ARTICLE
10.1002/2014GC005536

Chalcophile behavior of thallium during MORB melting and implications for the sulfur content of the mantle

Sune G. Nielsen[1], Nobumichi Shimizu[1], Cin-Ty A. Lee[2], and Mark D. Behn[1]

[1]Department of Geology and Geophysics, Woods Hole Oceanographic Institution, Woods Hole, Massachusetts, USA, [2]Department of Earth Science, Rice University, Houston, Texas, USA

Key Points:
- The ratio Ce/Tl is constant in MORB
- Ratio between sulfide and clinopyroxene is constant in the mantle
- DMM contains 195 ± 45 ppm sulfur

Supporting Information:
- Readme
- Table S1

Correspondence to:
S. G. Nielsen,
snielsen@whoi.edu

Citation:
Nielsen, S. G., N. Shimizu, C.-T. A. Lee, and M. D. Behn (2014), Chalcophile behavior of thallium during MORB melting and implications for the sulfur content of the mantle, *Geochem. Geophys. Geosyst.*, *15*, 4905–4919, doi:10.1002/2014GC005536.

Received 7 AUG 2014
Accepted 25 NOV 2014
Accepted article online 4 DEC 2014
Published online 18 DEC 2014

Abstract We present new laser ablation ICP-MS trace element concentration data for 28 elements in 97 mid-ocean ridge basalt (MORB) glasses that cover all major spreading centers as well as Tl concentration data for all mineral phases in five lherzolites from the Lherz massif, France. The ratio between the elements thallium (Tl) and cerium (Ce) is nearly constant in MORB, providing evidence that the depleted MORB mantle (DMM) has uniform Ce/Tl. Lherzolite mineral data reveal that sulfides are heterogeneous and contain between 23 and 430 ng/g of Tl while all other minerals contain Tl below the analytical detection limit of ~1 ng/g. We argue that Tl in MORB is controlled by residual sulfide during mantle melting. To investigate the observed relationship between Tl and Ce, we conduct models of fractional mantle melting, which show that the constant Ce/Tl in MORB is only reproduced if the ratio between clinopyroxene and sulfide in the upper mantle varies by less than 10%. In addition, the rate of melting for these two phases must be nearly identical as otherwise melt depletion and refertilization processes would lead to Ce/Tl fractionation. These model results allow us to establish a relationship for the sulfur content of DMM: $[S]_{DMM} = SCSS \times M_{cpx} / R_{cpx}$, where SCSS is the sulfur concentration of a silicate melt at sulfide saturation, R_{cpx} is the melt reaction coefficient, and M_{cpx} is the modal abundance of clinopyroxene in the DMM. Using this equation, we calculate that the average upper mantle sulfur concentration is 195 ± 45 μg/g.

1. Introduction

Thallium (Tl) isotopes are a relatively newly explored stable isotope system that show potential as a tracer of crustal components in igneous systems because of the highly fractionated isotopic signatures observed in low temperature altered oceanic crust [*Nielsen et al*., 2006a] and marine ferromanganese sediments [*Nielsen et al*., 2013; *Rehkämper et al*., 2002, 2004]. For example, studies have suggested that Tl isotopes in ocean island basalts (OIB) can trace the presence of recycled marine ferromanganese sediments in the mantle source [*Nielsen et al*., 2006b, 2007]. Additionally, Tl isotopes may prove to be an excellent tracer of inputs from the subducted slab to the mantle wedge [*Prytulak et al*., 2013].

One of the main difficulties when interpreting Tl isotope data in igneous rocks stems from the scarcity of knowledge about the geochemical behavior of this element during melting, fractional crystallization, and assimilation. Historically, Earth scientists have rarely analyzed Tl because of its low abundance in mantle-derived rocks. Therefore, most information on the Tl distribution in igneous systems originates from highly evolved rocks that tend to be substantially more enriched in Tl and hence more analytically tractable [*Heinrichs et al*., 1980; *Shaw*, 1952]. The abundance of Tl in the continental crust is controlled primarily by its univalent charge and large ionic radius, which is akin to the alkali metals potassium (K), rubidium (Rb), and cesium (Cs) [*Heinrichs et al*., 1980; *Shannon*, 1976; *Wedepohl*, 1974]. The large ionic radius is thought to render Tl highly incompatible during igneous processing and hence it concentrates in the continental crust [*Shaw*, 1952]. Some studies have also found that Tl is enriched in certain sulfides [*Heinrichs et al*., 1980; *Shaw*, 1952], which is a characteristic that was noted when Tl was first discovered [*Lamy*, 1862]. Since there is no mineral phase in the mantle that directly accommodates alkali metals, it is unclear what element Tl behaves most similarly to in this environment. Thallium isotope studies have suggested that correlations between Tl isotopes and the Cs/Tl ratio in OIB points toward a more alkali-like Tl affinity in the mantle [*Nielsen et al*., 2007, 2006b]. However, recent experimental work on the partitioning of Tl between sulfide and silicate melts indicates that Tl might be sequestered by sulfides [*Kiseeva and Wood*, 2013; *Wood et al*., 2008].

Given this seemingly contrasting evidence, we must first understand what processes govern the elemental distribution of Tl in primitive lavas before we can use Tl isotopes as a quantitative tracer in mantle-derived melts.

Here we perform the first global analysis of Tl concentration data in mid-ocean ridge basalts (MORB) with the aim of determining the geochemical behavior of Tl during mantle melting. We find that Tl is likely controlled primarily by sulfides in the mantle and we discuss the implications of this chalcophile behavior for the sulfur content of the depleted MORB mantle (DMM).

2. Methods and Samples

2.1. Samples Analyzed

We analyzed trace element concentrations in 97 MORB glasses (supporting information Table S1), 87 of which are from the Smithsonian collection [*Melson et al*., 2002] and 10 samples are from the Gakkel Ridge provided by Charlie Langmuir. We selected aphyric samples from most of the major spreading centers around the globe: East Pacific Rise, Juan de Fuca Ridge, American Antarctic Ridge, Mid-Atlantic Ridge, Central Indian Ridge, and Gakkel Ridge. All samples except three have >6% MgO in order to minimize potential effects from assimilation and/or fractional crystallization [*Rubin and Sinton*, 2008; *Wanless et al*., 2010].

We also analyzed Tl concentrations in the mineral phases olivine, orthopyroxene, clinopyroxene, spinel, and sulfide from five lherzolites (LN12-18A2B, LN12-18B2A, LN12-18B2B, LN12-18B2C, and LN12-18B2D) from the Lherz massif, France. Although lherzolites from Lherz do not represent primitive mantle [*Le Roux et al*., 2007, 2009], the trace element abundances of these lherzolites are likely similar to the upper mantle. For this reason, the Tl concentrations in the minerals should provide a reasonable illustration of the Tl distribution in the upper mantle. In general, mantle peridotites often contain two types of sulfide, one that is interstitial at grain boundaries and one that is included within silicate grains [*Alard et al*., 2002; *Burton et al*., 1999; *Harvey et al*., 2011; *Luguet et al*., 2003]. In Lherz, however, included sulfides are rare [*Lorand et al*., 2010] and are most frequently <20 μm in diameter, which makes it difficult to obtain precise Tl concentration data because the detection limit increases at smaller spot sizes. We, therefore, only analyzed interstitial sulfides for this study, which limits the ability to assess the influence of included sulfides on the Tl mass balance.

2.2. Trace Element Concentration Determination by Laser Ablation ICP-MS

Concentrations of 28 trace elements including Tl, Pb, Cs, Rb, La, and Ce were determined using a single-collector inductively coupled plasma sector field mass spectrometer (Thermo Finnigan Element 2 ICP-MS) at Rice University (supporting information Table S1). A New Wave 213 nm laser ablation system was used for sample introduction. The laser was operated with a fluence of 20 J/cm^2, a pulse frequency of 10 Hz, and a spot size of 110 μm, which was utilized in order to obtain the largest possible Tl ion beam and thus lower detection limit. Integration time on Tl and Cs was also increased from 0.01 to 0.03 s to improve counting statistics on these two elements. The elements K, P, Sc, V, Cr, Mn, Co, Ni, Cu, Zn, Ga, Y, and Zr were analyzed in medium ($m/\Delta m \sim 3000$) resolution mode, while the elements Cr, Mn, Co, Ni, Zn, Rb, Sr, Y, Zr, Nb, Cs, Ba, La, Ce, Gd, Yb, Lu, Hf, Ta, Tl, Pb, Th, and U were measured in low ($m/\Delta m \sim 300$) mass resolution mode. For each sample, either four or six separate laser analyses were conducted; two (or three) individual spots in low-resolution mode and two (or three) spots in medium resolution mode. Reported concentration data are therefore the average of several analyses. In all cases, the agreement between multiple spots as well as between elements analyzed in both low and medium resolution mode (i.e., Cr, Mn, Co, Ni, Zn, Y, and Zr) was better than the long-term reproducibility of the method.

Data reduction was performed by first subtracting the average gas background from the ablation signal. Instrumental drift and ablation efficiency were then accounted for by normalizing to an initial measurement using an internal standard. In this case, we used the known concentration of an element for normalization (^{25}Mg) that had previously been determined with an electron microprobe at the Smithsonian Institution [*Melson et al*., 2002]. Elemental concentrations were quantified by generating calibration curves from multiple analyses of the three USGS glass reference materials BIR-1G, BHVO-2G, and BCR-2G. These standards were chosen because they span the entire trace element concentration spectrum observed in MORB melts [*Nielsen and Lee*, 2013]. Calibration curves included standards analyzed before and after each sample mount

Table 1. Trace Element Concentrations in μg/g and Standard Deviation of Secondary Reference Materials

	VG-2	sd (%)	VG	sd (%)	A-99	sd (%)
n^a	20		12		7	
Rb	1.57	12.0	0.59	12.4	15.7	15.6
Cs	0.0169	10.5	0.0074	12.8	0.155	10.3
Ce	13.5	12.7	7.86	6.6	56.8	8.5
Tl	0.0120	13.4	0.0091	13.3	0.0324	12.5
Pb	0.53	10.9	0.48	4.1	1.77	7.2

[a]*n*—Number of analyses.

in order to correct for any secondary drift of the element/Mg ratio between standards and samples. These calibration curves always produced correlation coefficients of $R^2 > 0.98$, which shows that instrumental drift between samples and standards was very minor.

Samples were analyzed as glass chips mounted in 1 in. epoxy rounds. Most of the rounds contained one or several of three basaltic glass standards, A-99, VG, and VG-2. The repeatability of these reference materials (Table 1) represents our best estimate of the long-term external precision for the MORB glass analyses, which is about ±15% or better for all elements. Detection limits for all elements were defined as 3 times the average gas background determined prior to each analysis. During the MORB analyses, this approach yielded detection limits for Tl that was always better than 0.5 ng/g.

A second set of analyses was performed to investigate Tl concentrations in peridotite minerals from five lherzolite samples collected at the Lherz massif in the Pyrenees, France. Silicate minerals and spinel were analyzed using the same methods as for the MORB glasses, except that ^{57}Fe was used for normalization instead of ^{25}Mg. The Fe contents of each mineral phase were taken from previous analyses of lherzolites from Lherz that exhibited <10% variation [*Le Roux et al*., 2007], which shows that we are unlikely to induce significant uncertainties in our laser analyses by using an assumed Fe concentration. The detection limit for Tl during the lherzolite analyses were significantly higher than during the MORB measurements and were consistently around 1 ng/g.

For sulfides, the laser was operated with a fluence of only ~10 J/cm^2 in order to limit the ablation speed because sulfide is a much softer material than silicates and spinel. The pulse frequency was 10 Hz and spot sizes varied between 25 and 60 μm, depending on the size of the sulfide. The elements Mg, Fe, Ni, Co, Cu, Zn, Mo, Ag, Sn, Sb, Te, Ir, Tl, Pb, and Bi were monitored in low-resolution mode. Magnesium concentrations were not quantified and the Mg beam was only monitored in order to assess if the laser was ablating silicate minerals. The USGS reference sulfide MASS-1 was employed to construct calibration curves. We determined a Tl concentration for MASS-1 of 56.8 μg/g by conventional solution ICP-MS, which we used for our mass calibration curves. This value is in good agreement with the "information" Tl concentration of ~50 μg/g supplied by the USGS. As was the case for the major minerals, ^{57}Fe was used for normalization during data reduction. The detection limit for Tl in the sulfides varied significantly because of the variable spot sizes we were able to use. In general, detection limits for these analyses were between 1 and 10 ng/g.

Lherzolite minerals were analyzed in 150 μm thick sections. Each sulfide was imaged with a Bruker SEM prior to laser analysis. The concentrations of Fe, Ni, Cu, and S were quantified using the EDS detector on the Bruker SEM and the Fe contents were used as the internal standard. The concentrations of Ni and Cu determined by laser and EDS were always in reasonable agreement (Figure 1), which shows that, even though sulfides are clearly heterogeneous, the major element (only Ni was a major element in the analyzed sulfides) chemical compositions of each sulfide grain did not vary by more than ±25% (Figure 1). We are therefore only confident that sulfide trace element compositions are precise to within the same uncertainty because variation in the Fe content of the sulfides would propagate directly into the trace element concentrations.

3. Results

We present concentration data for 97 MORB glasses (all samples except three have MgO > 6%) covering the majority of spreading centers and chemical compositions (supporting information Table S1). We find that Ce/Tl is near constant (Ce/Tl ~ 1280 ± 430, 2 sd) for the entire range of geographical and chemical variability (Figure 2). In addition, Pb/Tl also shows little variation with ratios slightly higher (Pb/Tl ~ 60) for low Tl

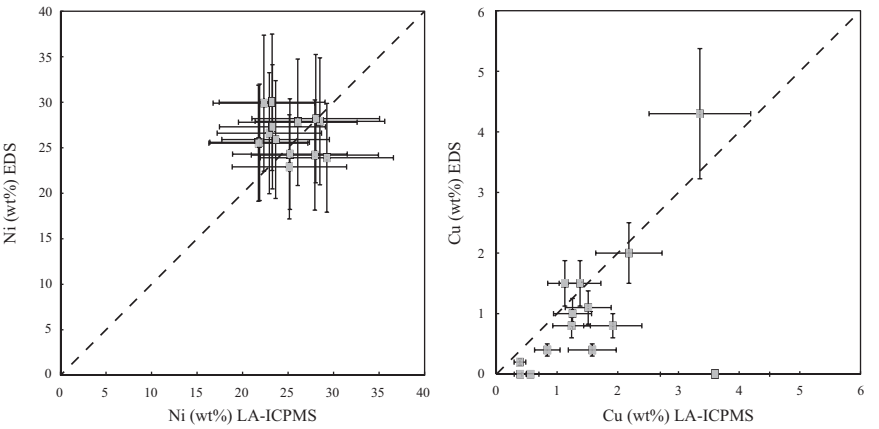

Figure 1. Nickel and copper concentrations in sulfides measured by EDS in the Bruker tabletop SEM and by laser ablation ICP-MS. The dashed line is the 1:1 line. Error bars of ±25% have been added for illustration purposes and show that, except for at Cu concentrations below ~2%, the SEM EDS system provides reasonable major element concentrations that can be used for internal normalization during laser ablation analyses.

concentrations than at higher Tl concentrations (Pb/Tl ~ 45) (Figure 2). The recent study of *Jenner and O'Neill* [2012] reports Tl concentration data for 497 MORB glasses (we have excluded MgO < 6 wt %, seamounts, back-arc basins and aseismic ridges from the original data set) none of which are the same as our samples analyzed here. Their data are consistent with our findings (Ce/Tl ~ 1180 ± 640, 2 sd), but they observe a wider spread in Ce/Tl at low Tl concentrations than we observe here (Figure 2). However, their measurements were done with a less sensitive mass spectrometer (Agilent quadrupole ICP-MS), which resulted in a detection limit up to an order of magnitude higher (2–6 ng/g) than we obtained in this study (~0.5 ng/g). Therefore, the lowest Tl concentration data of *Jenner and O'Neill* [2012] are likely to be somewhat less precise than our results, which provides a possible explanation for why they observe a larger spread in their data than we do at low Tl concentrations (Figure 2).

In the lherzolite samples, we analyzed a total of 28 clinopyroxene, 30 orthopyroxene, 6 olivine, and 5 spinel grains. None of the analyses were above the detection limit for Tl of 3 times the background, which on average was ~1 ng/g. Hence, all the major minerals of the five lherzolite samples contained <1 ng/g Tl. The sulfides, on the other hand, were all above detection limit and contained between 23 and 430 ng/g (Table 2) with an average of ~120 ng/g ($n = 14$).

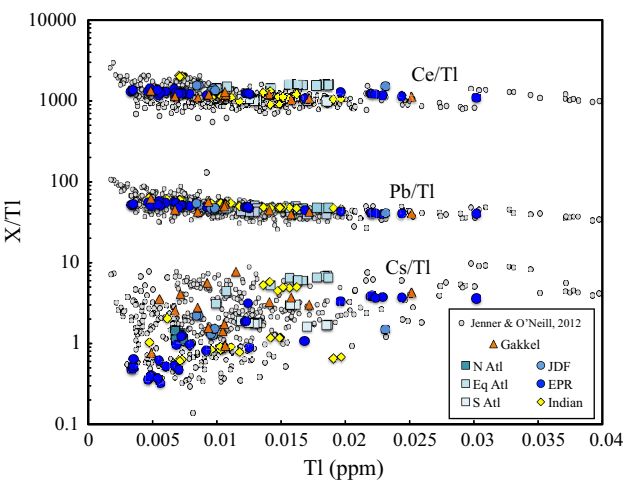

Figure 2. Ce/Tl, Pb/Tl, and Cs/Tl versus Tl concentration. Symbols are grouped by geographical region. Circles signify samples from the Pacific Ocean, where dark blue represents the East Pacific Rise (EPR) and light blue the Juan de Fuca Ridge (JDF). Squares signify samples from the Atlantic Ocean, beige is South Atlantic (S Atl), pale blue is Equatorial Atlantic (Eq Atl), and turquoise is North Atlantic (N Atl). Triangles signify samples from the Arctic Ocean (Gakkel). Diamonds signify samples from the Indian Ocean (Indian). Gray dots are MORB data from *Jenner and O'Neill* [2012]. Note the logarithmic scale on the *y* axis.

4. Discussion

4.1. Partitioning of Thallium in the Mantle

To quantify the relative partitioning behavior of Tl and other trace elements, we plotted the logarithm of Tl and other trace element concentrations against each other (Figure 3). In these diagrams, a slope of 1 signifies that the two elements have identical bulk partition coefficients ($k_D = D_{ol} \times M_{ol} + D_{opx} \times M_{opx} + D_{cpx} \times M_{cpx} + D_{sp} \times M_{sp} + D_{sulf} \times M_{sulf}$; where D_x is the mineral-melt partition coefficients for

Table 2. Sulfide Concentration Data Measured by LA-ICP-MS

Sample ID	LN12–18A2B-7	LN12–18B2A-16	LN12–18B2A-17	LN12–18B2B-7	LN12–18B2B-10	LN12–18B2C-2	LN12–18B2C-1	LN12–18B2C-6	LN12–18B2C-5	LN12–18B2D-5	LN12–18B2D-6	LN12–18B2D-7	LN12–18B2D-12	LN12–18B2D-3
Spot size micron	30	30	30	30	40	55	30	25	30	50	30	25	50	60
S wt % EDS	34.6	33.2	28.3	37	35.6	34.8	32.8	33.8	34.5	35.1	34.2	34.2	33.6	35.6
Ni wt % EDS	30	25.6	22.9	25.5	24.3	26.6	27.9	28.2	27.8	29.9	25.9	24.2	23.9	27.3
Fe wt % EDS	35.4	39.8	40.1	37	38.1	37.5	38	36.9	36.8	34.6	38.9	40.8	41	37.2
Cu wt % EDS	0	1.5	4.3	0.4	2	0.8	1.1	0.2	0	0.4	1	0.8	1.5	0
Co (wt %)	0.43	0.54	0.28	0.52	0.58	0.39	0.56	0.41	0.69	0.37	0.50	0.61	0.70	0.70
Ni (wt %)	23.2	21.9	25.1	21.7	25.2	22.9	28.5	28.0	26.1	22.3	23.6	27.9	29.3	23.3
Cu (wt %)	0.39	1.13	3.35	1.58	2.18	1.92	1.51	0.39	3.60	0.84	1.25	1.24	1.38	0.56
Zn (μg/g)	1.7	20.8	7.9	8.7	9.2	4.9	6.3	4.7	10.5	7.7	9.0	20.7	20.8	6.4
Mo (μg/g)	0.5	2.4		0.3	1.8	1.8	0.7	0.3	0.3	1.1	2.1	0.6	9.3	0.5
Ag (μg/g)	15.2	5.4	6.9	3.7	2.2	1.9	15.8	3.1	192.5	6.8	6.2	6.4	7.7	2.9
Sn (μg/g)	0.09	0.09	0.24	0.10	0.08	0.03	0.35	0.20	0.18	0.07	0.30	0.28	0.16	0.04
Sb (μg/g)	0.050	0.046	0.052	0.034	0.018	0.017	0.100	0.055	0.052	0.011	0.019	0.056	0.030	0.009
Te (μg/g)	0.9	3.0	9.8	7.5	1.7	3.2	2.2	12.0	1.3	6.4	2.7	2.8	1.4	2.9
Ir (μg/g)	0.24	0.92	0.86	3.03	0.22	0.65	0.10	0.17	0.64	1.04	2.26	0.05	1.15	0.92
Tl (μg/g)	0.296	0.113	0.032	0.159	0.096	0.092	0.092	0.047	0.426	0.048	0.154	0.093	0.048	0.023
Pb (μg/g)	4.4	7.9	1.1	23.8	2.2	2.2	2.6	4.1	18.0	10.4	8.7	9.4	13.3	3.9
Bi (μg/g)	0.46	1.44	0.18	0.56	0.35	0.14	0.29	0.74	1.79	1.33	0.34	0.34	0.57	3.25
Sum	59.1	63.5	68.8	60.8	66.0	63.3	68.6	65.8	67.4	58.6	64.4	70.8	72.3	61.5
Calculated wt % S[a]	40.9	36.5	31.2	39.2	34.0	36.7	31.4	34.2	32.6	41.4	35.6	29.2	27.7	38.5

[a]Sulfur concentration was calculated from the laser ablation data by assuming S accounted for the entire missing mass of the sulfide.

olivine, orthopyroxene, clinopyroxene, spinel, and sulfide and M_x is the mineral abundances by weight of the same minerals). Theoretically, it is possible to produce a slope of 1 in log-log plots of incompatible elements if large amounts of fractional crystallization were responsible for the majority of spread in concentrations. However, all MORB samples considered here contained >6% MgO and at any given MgO content we observe Tl concentration variations of more than a factor of 5 (not shown), which cannot be caused by fractional crystallization. We find that when combining all available MORB data, the slope for the diagram with log[Tl] and log[Ce] is 0.999 ± 0.034 (2 sd, n = 594), which indicates that these two elements partition identically during MORB melting (Figure 3). The two next closest elements are La, which is more incompatible than Tl and has a slope of 1.27, and Pb, which is slightly more compatible than Tl with a slope of 0.85. The slopes of these lines were calculated from York regressions [*York et al.*, 2004] of all MORB data (n = 594) where errors in both concentrations were taken into account. Our data set produces the same slope, but with a larger uncertainty due to the smaller number of samples (0.998 ± 0.094, 2 sd, n = 97). The uncertainties for La, Ce, and Pb were estimated to be about ±10% whereas uncertainties for Tl concentrations were assumed to increase with decreasing concentration. Specifically, we impose Tl uncertainties of ~10% above 20 ng/g, 14% at 10 ng/g, 20% at 6 ng/g, and 35% at 3 ng/g. These estimates are based on the repeat analyses over several analytical sessions of the glasses BIR-1G, BHVO-2G, A-99, VG, and VG-2 (Table 1), in which we observed uncertainties around 30–40% for measurements of BIR-1G ([Tl] = 2.5 ng/g, *Nielsen and Lee* [2013]) compared to 10–15% for the other glasses. We did not differentiate between analyses performed here and those of *Jenner and O'Neill* [2012] as we were only able to make quantitative error estimates for our

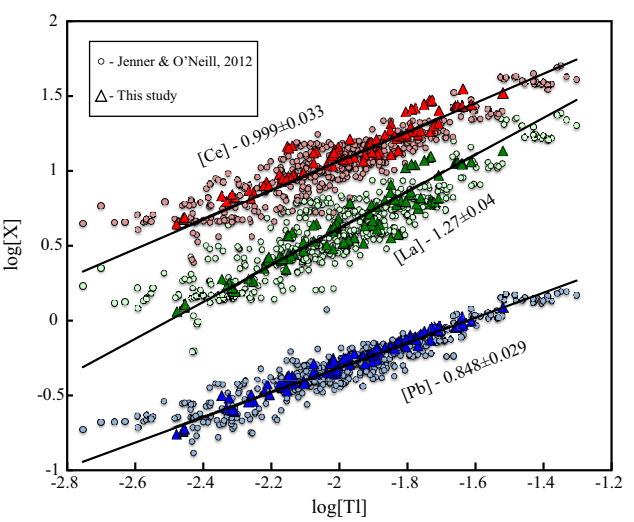

Figure 3. Logarithm of the Tl concentration versus the logarithm of the concentrations of Ce (red), La (green), and Pb (blue). Circles represent samples analyzed by *Jenner and O'Neill* [2012], triangles are from this study. In log-log plots of melt concentrations a slope of 1 signifies that the two elements partition identically during melting.

own analyses. However, there is no indication that, except for cases where *Jenner and O'Neill* [2012] were very close to detection limit, their uncertainties would exceed ours.

Given that Ce/Tl is constant in MORB, it is important to assess the relation between Ce/Tl in MORB and the depleted MORB mantle (DMM). In principle, extrusive MORB is not a direct reflection of the melt that was extracted from the upper mantle. Studies have shown that fractional crystallization, assimilation, and magma recharge may affect the compositions of MORB prior to eruption [*Lee et al*., 2014; *Rubin and Sinton*, 2008; *Wanless et al*., 2010]. However, fractional crystallization and magma recharge mainly affect trace element concentrations and not ratios between elements with similar bulk partition coefficients; in particular, highly incompatible elements are insensitive to such processes. Assimilation could significantly alter trace element ratios, but such effects have primarily been identified in relatively evolved MORB [*Wanless et al*., 2010] and here we only consider samples with >6% MgO. Since Tl and Ce are both strongly incompatible, we infer that the constant Ce/Tl ratio of MORB likely reflects that of the mantle source from which they were derived.

In order to estimate the average upper mantle Ce/Tl ratio, we use the slope and intercept as well as 2 sd uncertainties from the York regression shown in Figure 3. This approach produces a more robust estimate for the average upper mantle concentration because it takes the relationship between the measurement uncertainty and the Tl concentration into account. We obtain a best estimate for the upper mantle of Ce/Tl = 1110 ± 330 (2 sd), where the uncertainty is derived from the errors on the slope and intercept in Figure 3. This approach is preferred to conventional standard deviation because of the large errors associated with low Tl concentrations both in our data set and that of *Jenner and O'Neill* [2012].

Although Ce/Tl does not vary systematically with element concentration, it is clear that some variation in Ce/Tl exists outside analytical errors (Figure 2). This heterogeneity could be interpreted in several ways: (1) Ce/Tl in the upper mantle varies to some extent, (2) fractional crystallization, magma recharge, and assimilation induce small changes in Ce/Tl, and/or (3) minor variations in bulk partition coefficients of Ce and Tl, arising from mineralogical heterogeneity, cause Ce/Tl of melts to display small offsets from their mantle sources. While it is not presently possible to disentangle these processes, it is important to note that the combined effects are very minor, such that Ce/Tl displays similar variation in MORB as is observed for other constant trace element ratios like Rb/Cs, K/U, and Nb/U [*Hofmann et al*., 1986; *Hofmann and White*, 1983; *Jenner and O'Neill*, 2012]. We therefore focus on the strong evidence that for the *average* MORB mantle, Ce is the element that partitions most like Tl.

The identical k_Ds of Ce and Tl are surprising because the ionic radii and valence states of these two elements in the mantle are very different. In igneous processes, Tl is a very large univalent cation (~1.5 Å), similar to the alkali metals potassium (K), rubidium (Rb), and cesium (Cs) [*Shannon*, 1976], which are all highly incompatible during mantle melting. Thallium may also occur in the trivalent state, which would partition very differently to univalent thallium. However, thermodynamic data show that only at highly oxidizing conditions will significant amounts of Tl^{3+} form. Seawater, for example, which has an oxygen fugacity many orders of magnitude above any mantle source, possesses almost exclusively Tl^{+} [*Nielsen et al*., 2009a, 2011] and hence the redox chemistry of Tl is unlikely to play a role in the partitioning of Tl during mantle melting.

Our data reveal that ratios between Tl and the alkali metals exhibit almost two orders of magnitude variation in MORB (Figure 2). These data prove that although the ionic radii and charges of the alkali metals and Tl are essentially identical, they partition very differently into MORB melts. By contrast, Ce is a trivalent cation with an intermediate ionic radius (~1.0 Å), which makes it moderately incompatible during mantle melting due to its slight partitioning into clinopyroxene [*McDade et al*., 2003]. Thus, based on their ionic radii and charges, there is no obvious reason that Tl and Ce should partition identically during mantle melting.

Since the independent discoveries of Tl in 1861 by *Crookes* [1861] and A. Lamy, it has been known that this element forms two series of compounds: one that resembles alkali metals; the other similar to Pb with a strong affinity for sulfides [*Lamy*, 1862]. In addition, Tl has been shown to partition into sulfides and metals enriched in sulfur when equilibrated with silicate melts [*Kiseeva and Wood*, 2013; *Wood et al*., 2008]. The affinity of Tl for sulfide compounds is most likely related to its electron configuration whereby the outermost electron shell contains three electrons one of which is in the 6p orbital. This electron configuration tends to favor covalent bonds such as those occurring in sulfides. The alkali metals, on the other hand, all have a lone s-electron in the outermost shell, which tends to favor ionic bonding. With these chemical differences between Tl and the alkali metals in mind, it is therefore reasonable to infer that the larger-than-

Table 3. Mineral-Melt Coefficients Used in Melting Model

	DMM[a] (μg/g)	$D_{cpx/melt}$	$D_{opx/melt}$	$D_{ol/melt}$	$D_{sp/melt}$	$D_{sulf/melt}$
Tl[b]	0.00048	0.0006	0.00045	0.000045	0	Model
Ce[c]	0.55	0.14	0.006	0.00004	0	0
Pb[d]	0.025	0.01	0.003	0.00001	0	Model

[a]Concentration of Ce in DMM from *Workman and Hart* [2005], while those of Pb and Tl are based on the Ce/Tl and Pb/Tl ratios observed for DMM, where it is assumed that low Tl concentrations on average reflect the highest degree of melting and hence the DMM Ce/Tl and Pb/Tl ratios.

[b]Tl partition coefficients in silicate minerals assumed identical to Rb due to their almost identical ionic radius and charge. Values taken from *Donnelly et al*., [2004].

[c]Ce partition coefficients from *McDade et al*. [2003], except spinel and sulfide, which are assumed.

[d]Pb partition coefficient in cpx from *Watson et al*. [1987]; orthopyroxene and olivine from *Kelemen et al*. [2003]. Spinel assumed.

expected Tl bulk partition coefficient during MORB melting is related to partitioning into sulfides. This interpretation is also supported by the narrow range of Pb/Tl ratios displayed by our samples (Figure 2), which suggests that Pb and Tl are controlled by the same mineral phase, namely sulfide.

The inferences made from global MORB data are also consistent with our LA-ICP-MS analyses of silicates, spinel, and sulfides in lherzolites. The only mineral that exhibited Tl concentrations above the detection limit was sulfides, which contained on average at least 100 times more Tl than did the major mineral phases (Table 2). While our data clearly show that sulfide is the mantle mineral that is characterized by the highest Tl concentrations, we are not able to show that sulfide is the *only* mineral that contributes to the Tl budget in the mantle. This shortfall is due to the low bulk Tl concentration of ~0.5 ng/g inferred for the upper mantle (Table 3). Thus, even if the silicate phases contained on average 0.2 ng/g of Tl (significantly below our detection limit of ~1 ng/g) that would still constitute almost 50% of the bulk lherzolites.

We did not attempt to determine the bulk Tl concentrations in our lherzolites by conventional solution ICP-MS because these samples showed clear signs of secondary alteration. It is well known that Tl is highly concentrated in secondary minerals during alteration [*Jochum and Verma*, 1996; *Nielsen et al*., 2006a, 2009b] and therefore bulk chemical analysis of our lherzolites would not enable us to determine if the entire Tl budgets were contained in sulfides or not. Assuming that the unaltered bulk lherzolites contain ~0.5 ng/g Tl (Table 3) and that the abundance of sulfide in these peridotites are about 0.06 wt % (equivalent to about 200 μg/g sulfur or 0.04 vol % sulfide), which is similar to other lherzolites at Lherz [*Lorand*, 1991], the sulfides would be predicted to display concentrations around 750 ng/g of Tl. The predicted thallium concentration is somewhat higher than the average concentrations measured here of ~120 ng/g (Table 2). This disagreement might suggest that a significant amount of the Tl in the lherzolites is located in the major mineral phases. There could, however, be several alternative explanations for this discrepancy. First, it is possible that we have over or underestimated the bulk Tl concentration or sulfide abundance, respectively, in our samples. If the bulk Tl content was closer to 0.1 ng/g and the sulfide abundance was 0.1 wt %, then the sulfides readily account for all the Tl in the samples. Second, as outlined in the sample description section, we have only analyzed interstitial sulfides because these were analytically tractable. If Tl concentrations for included sulfides are significantly higher than interstitial sulfides, as has been observed for Os [*Harvey et al*., 2011], then the included sulfides might account for the observed Tl deficit. However, this would not be expected given that included sulfides are rare at Lherz [*Lorand et al*., 2010] and because Os is far more compatible in liquid sulfide than is Tl [*Brenan*, 2008; *Kiseeva and Wood*, 2013]. Third, it has been shown experimentally that Tl, like many other mildly chalcophile elements, is incompatible when sulfides crystallize from sulfide melts [*Jones et al*., 1993; *Li and Audetat*, 2012]. This behavior readily explains why we observe more than an order of magnitude variation in the Tl contents of our sulfides because different sulfides may represent different stages of sulfide crystallization. By the same token, Tl might be expected to concentrate in the last droplets of sulfide melt that crystallize during peridotite cooling. These final sulfide melts would be expected to preferentially exist along sulfide grain boundaries, which constitute the portion of the sulfides we have sampled the least with our laser analyses. It is possible that the same explanation accounts for the lower-than-expected Pb concentrations often recorded for mantle sulfides [*Blusztajn et al*., 2014; *Burton et al*., 2012; *Warren and Shirey*, 2012].

Taken together, the evidence from MORB glasses, peridotite minerals, and the ionic size and charge of Tl strongly suggest that sulfides are, if not the only Tl reservoir in the mantle, then at least the most significant.

Given that all current evidence points toward sulfides as the dominant reservoir for Tl in the mantle, in the following we discuss some interesting implications that arise from the constant ratio between Tl and Ce in MORB.

4.2. Fractional Melting Models of MORB Ce/Tl

It is well known that Ce in MORB is controlled by clinopyroxene [*McDade et al*., 2003], so if Tl is controlled primarily by sulfide, the bulk partition coefficients of Tl and Ce can be approximated as $k_{D,Tl} = M_{sulf} \times D_{sulf,Tl}$ and $k_{D,Ce} = M_{cpx} \times D_{cpx,Ce}$, where M_{sulf} and M_{cpx} are the upper mantle modal abundances of sulfide and clinopyroxene, respectively, and $D_{sulf,Tl}$ and $D_{cpx,Ce}$ are the mineral partition coefficients for Tl in sulfide and Ce in clinopyroxene, respectively. Given that $k_{D,Tl} \sim k_{D,Ce}$ (Figure 3), we rewrite these expressions such that $M_{sulf}/M_{cpx} = D_{cpx,Ce}/D_{sulf,Tl}$. Although element partition coefficients may vary with temperature, pressure, and mineral/melt composition, for simplicity we assume that $D_{cpx,Ce}$ and $D_{sulf,Tl}$ can be considered constant for normal MORB melting. Therefore, it follows that the ratio between sulfide and clinopyroxene in the upper mantle cannot vary substantially as otherwise Ce/Tl in MORB would not be as invariant as is observed.

In the following, we explore the conditions under which we can reproduce the ranges of Ce/Tl in our data (Figure 2) by calculating trace element partitioning assuming fractional, nonmodal mantle melting. We calculated fractional melting for melt increments of 0.1% up to a maximum of 16% melting. The mineral-melt reaction coefficients for clinopyroxene, orthopyroxene, spinel, and olivine were assigned values of 0.8, 0.32, 0.08, and −0.2, respectively—similar to the experimental values determined on peridotite at 1 GPa [*Baker and Stolper*, 1994; *Wasylenki et al*., 2003], but with a slightly higher melt reaction coefficient for clinopyroxene to account for the somewhat higher average pressure of MORB melting [*Kinzler and Grove*, 1992; *Klein and Langmuir*, 1987; *Longhi*, 2002]. Positive reaction coefficients denote that the mineral is consumed during melting while negative coefficients denote that the mineral is precipitated. All coefficients were assumed to be constant when all four phases were present (i.e., until clinopyroxene was exhausted at ∼16% melting at which point the calculation was stopped).

Sulfide removal followed the sulfur concentration in sulfide saturated basaltic melts (SCSS) and was set at 1200 μg/g S [*Liu et al*., 2007; *Mavrogenes and O'Neill*, 1999; *O'Neill and Mavrogenes*, 2002]. Sulfide solubility has previously been found to vary significantly as a function of temperature, pressure, and iron content of the melt [*Liu et al*., 2007; *Mavrogenes and O'Neill*, 1999; *O'Neill and Mavrogenes*, 2002; *Wallace and Carmichael*, 1992] and therefore we assumed that MORB melting on average takes place at the same temperature and pressure (1350°C, 1.5 GPa) generating melts with about 10% FeO [*Gale et al*., 2013]. In addition, we did not take into account that sulfides could exist as two distinct phases in the mantle: one that is interstitial and one that is included in silicate minerals [*Alard et al*., 2002; *Harvey et al*., 2011; *Luguet et al*., 2003]. It has been shown that these two sulfide phases in some peridotites contain different Pb, Re, and Os concentrations as well as Pb and Os isotope compositions [*Alard et al*., 2002; *Burton et al*., 2012; *Harvey et al*., 2011] and thus play a significant role in setting the Pb and Os isotope systematics of mantle-derived melts. If interstitial and included sulfides have highly different Tl concentrations, then the relative proportions of interstitial and included sulfides may affect the rate of Tl release into a melt and thereby the Ce/Tl ratio. Unfortunately, it is very difficult to perform quantitative modeling of this phenomenon, because several unconstrained parameters are required to calculate the effects of two distinct petrographic sulfide phases in the mantle. These parameters include: relative proportions of the two sulfide phases in the upper mantle, Tl concentrations in the two sulfide phases, and the relative proportions of the included sulfides in the different silicate phases (olivine included sulfides will be more difficult to release into the melt than clinopyroxene included sulfides). While detailed sulfide petrography exists for a good number of peridotites [*Lorand*, 1989, 1991; *Lorand et al*., 2010; *Luguet et al*., 2003] it is difficult to assess how relevant these sulfide distributions in peridotites are for the average upper mantle. In addition, all of our sulfide Tl concentration analyses were for interstitial sulfides and thus it is not possible with our data set to assess if sulfide petrography has an impact on Ce/Tl ratios of MORB. We note that the concentration difference between interstitial and included sulfides must largely depend on the partition coefficient between silicate melt and liquid sulfide, where the partition coefficients that most strongly favor liquid sulfide will tend to produce the largest difference between interstitial and included sulfides. With the relatively mildly chalcophile nature of Tl in mind [*Kiseeva and Wood*, 2013], one might, therefore, not expect a large Tl concentration contrast to exist

between interstitial and included sulfides. However, only future detailed investigations of Tl concentrations in mantle sulfides will resolve this question.

For our calculations, the modal abundances (by volume) of the minerals in unmelted DMM were cpx = 13%, opx = 28%, ol = 57%, sp = 2% [*Workman and Hart*, 2005]. When converted to fractions by weight (necessary in order to apply partition coefficients) these values change slightly to about cpx = 13.4%, opx = 27.2%, ol = 57.1%, sp = 2.2%. In the model runs variable amounts of sulfide were added to DMM, which required that the major minerals, together with sulfide, be renormalized to 100%. This renormalization had no significant effect on the mineral modes because sulfide was present at very low abundances (<0.1% by weight). In order to convert the abundance of sulfide into sulfur concentrations, we used 36% as the average S concentration in mantle sulfides, which assumes that mantle sulfides contain primarily Fe and Ni as cations. Mineral-melt partition coefficients used for Ce, Pb, and Tl are shown in Table 3 together with the concentrations of each element in DMM. The partition coefficients used for Tl in silicates were assumed to be similar to those of Rb because of the almost identical charge and ionic ratio for these two elements [*Shannon*, 1976]. The concentration of Tl in DMM is calculated based on the Ce/Tl ratio in MORB and assuming $[Ce]_{DMM} = 0.55$ μg/g [*Workman and Hart*, 2005]. It should be noted that other estimates exist for $[Ce]_{DMM}$ [*Kiseeva and Wood*, 2013; *Salters and Stracke*, 2004] that differ significantly from that of *Workman and Hart* [2005] and thus would serve to change the calculated Tl concentration of DMM. However, the results of our models only depend on the relative partitioning of Ce and Tl, and we adjust the partition coefficient of thallium in sulfide ($D_{Tl,sulf\text{-}sil}$) at different mantle sulfur abundances to achieve constant Ce/Tl. In reality, there are also significant uncertainties on Ce mineral partition coefficients as well as the modal mineralogy of the mantle, both of which will affect bulk partitioning of Ce and thereby also that of Tl (when using the inference that these two elements partition the same during mantle melting). However, these uncertainties will only affect the absolute $D_{Tl,sulf\text{-}sil}$, which is the reason we have kept this parameter free during our model runs.

4.2.1. Melt Depletion at Different Sulfur Concentrations

We modeled three different scenarios with variable mantle S contents (Figure 4). For each model simulation, the modal abundance of sulfide was chosen and subsequently the sulfide-silicate melt partition coefficients of Pb and Tl were adjusted until a best fit with Ce/Tl and Pb/Tl in MORB (Figure 2) was obtained. Sulfide/silicate melt partition coefficients found for Pb and Tl range from 22–120 to 18–100, respectively, when bulk S was between 79 and 400 μg/g. These ranges are in reasonable agreement with experimental determinations, which exhibit values for a large range of melt compositions of $D_{Tl,sulf\text{-}sil} = 4–24$ [*Kiseeva and Wood*, 2013] and $D_{Pb,sulf\text{-}sil} = 6–93$ [*Kiseeva and Wood*, 2013; *Lagos et al*., 2008; *Li and Audetat*, 2012]. The range in degree of melting for MORB indicated in Figure 4 covers the values estimated for normal (N-) MORB [*Hofmann*, 1988; *Klein and Langmuir*, 1987], transitional (T-) MORB [*Shaw et al*., 2010], and enriched (E-) MORB [*Donnelly et al*., 2004]. It should be noted that although E-MORB is likely produced by total degrees of melting similar to N-MORB, their enriched incompatible trace element signatures are thought to originate from incorporation of very low degrees of melting down to 0.2% that produced the E-MORB source [*Donnelly et al*., 2004]. If this particular model of E-MORB generation is correct, then E-MORB will record any fractionation of Ce/Tl and Pb/Tl that occurs at these low degrees of melting.

Based on this assumption, we can compare the calculated Ce/Tl ratio to the observed ratio over a wide range of F from ~1% to 16% (Figure 4). If we apply the definition of E-MORB (Ce > 25.2 μg/g) recently proposed by *Gale et al*., [2013], then we have 15 E-MORB samples from the East Pacific Rise, Mid-Atlantic Ridge, Gakkel Ridge, and Juan de Fuca Ridge within our data set and there are an additional 29 E-MORB samples in the data set of *Jenner and O'Neill* [2012]. None of these samples display fractionated Ce/Tl compared with more depleted samples from the same regions (supporting information Table S1). We therefore conclude that Ce/Tl is not fractionated by the very low degrees of melting that likely created the E-MORB sources [*Donnelly et al*., 2004]. Using these "low" degree melts as a constraint, we show that M_{sulf}/M_{cpx} cannot vary by more than ±10% in order to insure that the calculated Ce/Tl ratio does not exceed the data range (Figure 4b).

4.2.2. Refertilization and Melt Depletion Models

A second set of models was performed to investigate the effects on Ce/Tl in melts that originate from mantle volumes that have been refertilized by melt impregnation or previously depleted by melt removal. In these models we used the same mantle starting compositions as those shown in Figure 4a with sulfur

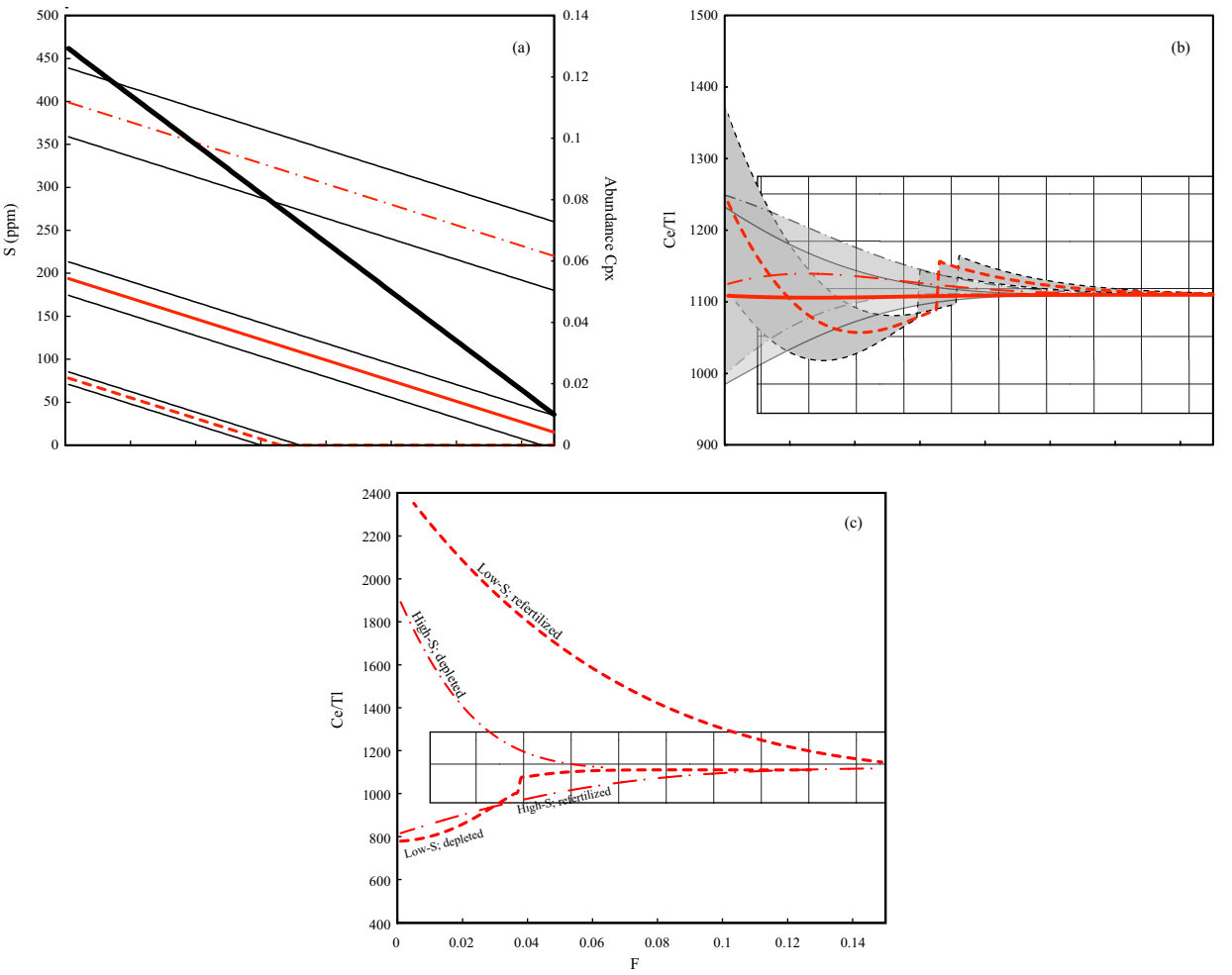

Figure 4. Modeled sulfide and clinopyroxene abundances (a) and Ce/Tl ratios (b and c) plotted against degree of melting (F). We modeled three different scenarios where the DMM contains 79 μg/g (dashed red lines), 195 μg/g (bold red lines), and 400 μg/g (dash-dot red lines) sulfur. In Figure 4b, we adjusted the partition coefficient of Tl in sulfide until a best fit with Ce/Tl in MORB was achieved. Lower sulfide requires a higher partition coefficient such that $D_{Tl,sulf}$ was 100, 36, and 18 for sulfur concentrations of 79 μg/g, 195 μg/g, and 400 μg/g, respectively. In each scenario, we then varied the sulfide abundance by $\pm$10% while keeping the best-fit $D_{Tl,surf}$ constant in order to generate the error envelopes around the red lines. In Figure 4c, we investigated Ce/Tl ratios in melts generated from mantle reservoirs that had been refertilized or depleted via melt rock reactions. Square grids in Figures 4b and 4c show the average Ce/Tl of global MORB with a 1 sd error envelope. MORBs extruded on the seafloor likely represent melting degrees between 5% and 15% [*Hofmann*, 1988; *Klein and Langmuir*, 1987]. However, the sources of enriched MORB (E-MORB) have trace element patterns that are thought to originate from very low (<1%) degrees of melting [*Donnelly et al.*, 2004], which we include for the purposes of constraining our model results (see text for more details).

concentrations of 79, 195, and 400 μg/g. For refertilization, each mantle reservoir was impregnated with 20% by volume of a melt generated from a second identical mantle reservoir. The new refertilized mantle mineral modes were calculated based on the same melt reaction coefficients used to generate the melt (i.e., clinopyroxene = 0.8, orthopyroxene = 0.32, spinel = 0.08, and olivine = −0.2) as well as the sulfur concentration of MORB melts, which is ~1200 μg/g [*Liu et al.*, 2007; *Mavrogenes and O'Neill*, 1999; *O'Neill and Mavrogenes*, 2002]. This process does not alter the mantle Ce/Tl ratio because the melts that cause the refertilization have the same Ce/Tl as the mantle source. However, depending on the initial amount of S in the mantle, the refertilized mantle will be characterized by different M_{sulf}/M_{cpx} ratios, which will cause melts generated from the refertilized mantle to be fractionated in Ce/Tl (Figure 4c). Only when the rate of sulfide and clinopyroxene removal is nearly identical will refertilization not result in a fractionation of M_{sulf}/M_{cpx}, which in turn will leave Ce/Tl constant in the subsequently extracted melt.

The melt depletion models shown in Figure 4c were generated by removing 3% melt from the low sulfur mantle and 10% melt from the high sulfur mantle. We chose these melt depletion degrees in order to preserve the ability to produce sulfur saturated melts from the depleted mantle. Melting is assumed to shut down when clinopyroxene is exhausted from the mantle residue, which is the reason the curves for melt

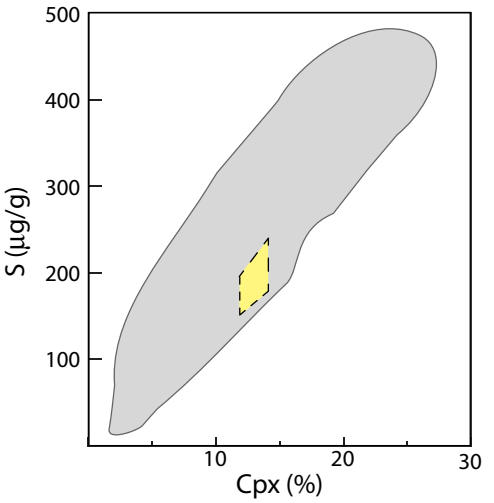

Figure 5. Modal abundance of clinopyroxene plotted versus S concentration in μg/g. Gray shaded area denotes data from 58 natural orogenic peridotite xenoliths [*Lorand*, 1989], whereas the yellow quadrangle shows our 1 sd area of $[S]_{DMM}$.

depletion end at ~6.5% and ~12.5% melting for the high and low sulfur reservoirs, respectively. Melt depletion produces similar fractionations of M_{sulf}/M_{cpx}, which again causes Ce/Tl fractionation in subsequent melting events.

It is important to note that continued cycles of refertilization and melt depletion, which are likely common in the mantle, will cause Ce/Tl to evolve away from the starting value because the magnitude of Ce/Tl fractionation is different for depletion and refertilization at any given S content (Figure 4c). Hence, it is not possible that refertilization and melt depletion will cancel out the induced fractionations of Ce/Tl.

Given the constraints of the models presented in Figure 4c, the constant Ce/Tl observed for MORB (Figure 2) is obtained only if the ratio between clinopyroxene and sulfide is essentially constant in the mantle. This result is consistent with the strong positive covariation observed between sulfur concentrations (and thereby sulfide) and clinopyroxene abundances in peridotites [*Lorand*, 1989] (Figure 5).

4.3. Potential Model Uncertainties

The main ambiguities in these model calculations arise from the fact that only the silicate mineral partition coefficients of Ce have been extensively investigated [*McDade et al.*, 2003]. Reliable partitioning data for Tl, and to some extent Pb, during MORB melting is scarce. Importantly, Tl and Pb partition coefficients in excess of 0.02 for clinopyroxene, orthopyroxene, or olivine would render silicates a major reservoir of Pb and Tl in the mantle. The only experimental study that investigated Tl partition coefficients for mantle minerals used hydrous basanite melts and was only able to assert that D_{Tl} for olivine, orthpyroxene, and clinipyroxene were <0.015 [*Adam and Green*, 2006]. Considering these uncertainties, and the fact that partition coefficients for hydrous melts are likely significantly different to anhydrous melts [*Blundy and Wood*, 2003], it is clear that, although the existing experimental data does not indicate Tl is more compatible in silicates than is Rb, we cannot presently exclude this possibility. More information is available on Pb partitioning with several experimental studies reporting coefficients for clinopyroxene. However, these studies found partition coefficients for Pb in clinopyroxene between 0.01 and 0.1 [*Hart and Dunn*, 1993; *Salters et al.*, 2002; *Watson et al.*, 1987], the higher end of which would make Pb controlled by a combination of both clinopyroxene and sulfide. For the purposes of our model, it is important to note that if Tl was also incorporated into silicates the required partition coefficient for Tl in sulfide would be smaller and consequently render the expression $M_{sulf}/M_{cpx} = D_{cpx,Ce}/D_{sulf,Tl}$ incorrect.

Based on the assertion by *Kiseeva and Wood* [2013] that the Fe content of a melt is the primary controlling parameter for chalcophile element partitioning into sulfide melt, these authors predict that $D_{Tl,sulf\text{-}sil} \sim 15$ and $D_{Pb,sulf\text{-}sil} \sim 40$ for MORB melts. This set of sulfide partition coefficients, however, is not able to reproduce the observed Pb/Tl ratios of MORB, unless Tl partitions more strongly into silicates than does Rb. As outlined above, this conclusion is certainly possible and future studies will need to investigate the exact partitioning behavior of Tl in mantle silicates. On the other hand, the experiments by *Kiseeva and Wood* [2013] were performed without appreciable amounts of Cu compared with mantle sulfide that likely contain several weight % Cu, which could have an effect on elemental partitioning. In addition, the relationship between $D_{Tl,sulf\text{-}sil}$ and FeO in silicate liquid is not well defined [*Kiseeva and Wood*, 2013], perhaps because $D_{Tl,sulf\text{-}sil}$ also depends on other parameters besides FeO in the silicate melt.

5. The Sulfur Concentration of the Upper Mantle

With the uncertainties for partitioning of Tl during mantle melting in mind, it is clear that the conclusion of a constant ratio between sulfide and clinopyroxene in the mantle, as well as the essentially identical

Table 4. Parameters Used for Calculation of $[S]_{DMM}$

Parameter	Value	Error	References
SCSS	1200 μg/g	150 μg/g	*Liu et al*. [2007], *Mavrogenes and O'Neill* [1999], *O'Neill and Mavrogenes* [2002], and *Wallace and Carmichael* [1992]
R_{cpx}	0.8	0.1	*Baker and Stolper* [1994], *Falloon and Green* [1987], and *Kinzler* [1997]
M_{cpx}	13%	2%	*Niu* [2004] and *Workman and Hart* [2005]

removal rates of these two minerals during melting, must be viewed with some caution. However, if our inference that sulfide is the only mantle mineral that contains significant amounts of Tl is correct then we can use the relationship between sulfide and clinopyroxene to put constraints on the sulfide content of the DMM.

Sulfur incorporation in silicate melts takes place above the sulfide liquidus [*Bockrath et al*., 2004] and the sulfur content of MORB is thus a function of sulfide melt solubility in silicate melts [*Liu et al*., 2007; *Mavrogenes and O'Neill*, 1999]. Therefore, we can write $[S]_{DMM} = SCSS \times F_{FeS,out}$, where SCSS is the sulfur concentration of a silicate melt at sulfide saturation and $F_{FeS,out}$ is the fraction of melting required to exhaust sulfide in the DMM. $F_{FeS,out}$ is not well constrained and thus it is not possible to use this equation directly. On the other hand, clinopyroxene is exhausted from the mantle via melt reactions such that $F_{cpx,out} = M_{cpx}/R_{cpx,}$ where $F_{cpx,out}$ is the fraction of melting required to exhaust clinopyroxene in the DMM and R_{cpx} is the melt reaction coefficient that determines the rate at which clinopyroxene is removed during melting. Based on the invariant Ce/Tl of MORB and the consistent covariation between sulfur and clinopyroxene in orogenic peridotites (Figure 5), we infer that clinopyroxene and sulfide melt out at the same rate and are therefore exhausted at the same degree of melting. We can thus substitute $F_{cpx,out}$ for $F_{FeS,out}$, producing the relationship:

$$[S]_{DMM} = SCSS \times M_{cpx}/R_{cpx} \quad (1)$$

Each of these parameters has been the subject of multiple investigations [*Baker and Stolper*, 1994; *Falloon and Green*, 1987; *Kinzler*, 1997; *Liu et al*., 2007; *Mavrogenes and O'Neill*, 1999; *Niu*, 2004; *O'Neill and Mavrogenes*, 2002; *Wallace and Carmichael*, 1992; *Workman and Hart*, 2005] and we are therefore able to plug reasonable values into equation (1) and obtain an independent estimate of the sulfur abundance of DMM. In Table 4, we list the best estimates for each parameter and their associated errors. From these we obtain a value of $[S]_{DMM} = 195 \pm 45$ (sd) μg/g. We have plotted the S concentration space outlined by our solutions to equation (1) in a diagram together with orogenic mantle peridotite data [*Lorand*, 1989], which reveals that our estimate of $[S]_{DMM}$ is completely encompassed by the orogenic mantle peridotite data (Figure 5). The strong coherence between the models and peridotite data, which are independent of each other, gives additional confidence that our value provides a rigorous assessment of $[S]_{DMM}$.

Our calculated $[S]_{DMM}$ provides evidence for the likely range of degrees of melting and the saturation state of sulfide in MORB. With $SCSS = 1200 \pm 150$ μg/g it is evident that sulfide is not exhausted from DMM until $\sim 16 \pm 5\%$ melting (Figure 4). It therefore follows that any MORB generated by less than $\sim$16% melting will be sulfide saturated. Since most MORB are thought to be sulfur saturated [*Wallace and Carmichael*, 1992], our $[S]_{DMM}$ estimate is in good agreement with models of MORB generation, which predict maximum extents of melting for MORB between 6% and 20% [*Asimow et al*., 2001; *Hofmann*, 1988; *Kinzler and Grove*, 1992; *Klein and Langmuir*, 1987].

6. Outlook for Deep Sulfur Cycling and Mantle Heterogeneity

In summary, the constant Ce/Tl ratio of MORBs appears to require that the melting rates of clinopyroxene and sulfide are synchronized in the upper mantle. This allows us to estimate the sulfide and hence bulk S content of the average depleted MORB mantle to be $\sim$195 μg/g. Given that it is primarily the ratio between sulfide and clinopyroxene that controls the Ce/Tl of melts, mineralogical heterogeneity of the upper mantle in the form of coupled enrichment or depletion of these two minerals would not be detectable by using Ce/Tl. Therefore, it should be stressed that Ce/Tl cannot be utilized to investigate sulfide heterogeneity of the mantle unless the ratio between sulfide and clinopyroxene has been disturbed by other processes than melting and refertilization, which appear to leave the ratio between sulfide and clinopyroxene unaffected.

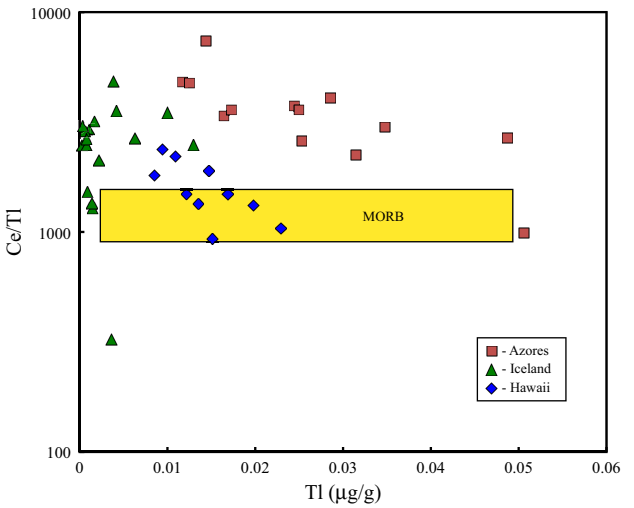

Figure 6. Ce/Tl versus Tl concentration for Hawaii, Iceland, and the Azores compared with MORB. While Ce/Tl in MORB does not vary significantly as a function of Tl concentration, all three OIBs show a substantial spread with Ce/Tl almost universally higher than MORB. For Hawaii and the Azores there is a suggestion of higher Ce/Tl at lower Tl concentrations, which could imply that the bulk partition coefficient for Ce is higher than Tl for these OIBs. In turn, this relationship is equivalent to higher clinopyroxene/sulfide ratios in the Hawaii and Azores mantle sources than in MORB. Thallium and cerium concentration data from *Nielsen et al.*, [2006b, 2007] and *Norman and Garcia* [1999].

Once transported deep into the mantle, recycled oceanic crust, and sediments are highly unlikely to be characterized by sulfide/clinopyroxene that is close to that of the upper mantle. For example, sediments often have very high S concentrations due the presence of diagenetic pyrite and altered oceanic crust has highly variable S concentrations due to remobilization during hydrothermal activity. On the other hand, calcium, the primary cation for clinopyroxene, is much less mobile during hydrothermal activity and completely decoupled from any of the processes governing S distributions in sediments and altered oceanic crust. In addition, subduction processes such as release of fluids from the slab into the mantle wedge will have very variable S/Ca ratios depending on oxygen fugacity, which again is likely to perturb the ultimate sulfide/clinopyroxene ratio of the deeply subducted material. Volcanism sourced from recycled crustal material (i.e., ocean island basalts and large igneous provinces) is therefore not expected to conform to the same invariance of Ce/Tl versus [Tl] as observed for MORB. The limited amount of Tl concentration data for ocean island basalts indeed displays more variation than MORB (Figure 6) with data from Hawaii and the Azores showing increasing Ce/Tl at decreasing Tl concentrations. These correlations are suggestive of lower sulfide/clinopyroxene in the Hawaii and Azores mantle sources than DMM, which could be consistent with pyroxenite in the source of Hawaii [*Sobolev et al.*, 2005] as long as these mantle sources contain less than 1500 μg/g of S. However, there could also be several other explanations for the variable Ce/Tl in OIB. First, Ce/Tl ratios in recycled oceanic crust are unlikely to be identical to the mantle, which would render OIB mantle sources heterogenous with respect to Ce/Tl. Second, systematic variations in the Tl concentrations between interstitial and included sulfides could also give rise to variable Ce/Tl, especially at the low degrees of melting often inferred for OIB [e.g., *Mckenzie and Onions*, 1991]. Given these uncertainties, it is currently speculative to infer the reasons for the observed variation in Ce/Tl for OIB.

Acknowledgments

The data for this paper are available in tables within the manuscript, in the online supporting information and can also be requested directly from the corresponding author: snielsen@whoi.edu. We are grateful for insightful and thorough reviews by Jason Harvey, Kate Kiseeva, and John Lassiter as well as the editorial handling by Janne Blichert-Toft. We acknowledge funding from NSF grant EAR 1119373 to SGN and an award from the WHOI Deep Ocean Exploration Institute to SGN and NS and funding from the Deep Carbon Observatory to MDB. We thank Veronique Le Roux for access to lherzolite samples from Lherz and Horst Marschall for allowing us to use his Bruker tabletop SEM. We gratefully acknowledge access to samples from the Smithsonian Institution and Charlie Langmuir. We also thank Charlie Langmuir and his group for comments on an earlier version of this manuscript.

References

Adam, J., and T. Green (2006), Trace element partitioning between mica- and amphibole-bearing garnet lherzolite and hydrous basanitic melt. 1: Experimental results and the investigation of controls on partitioning behaviour, *Contrib. Mineral. Petrol.*, *152*, 1–17.

Alard, O., W. L. Griffin, N. J. Pearson, J. P. Lorand and S. Y. O'Reilly (2002), New insights into the Re-Os systematics of sub-continental lithospheric mantle from in situ analysis of sulphides, *Earth Planet. Sci. Lett.*, *203*, 651–663.

Asimow, P. D., M. M. Hirschmann, and E. M. Stolper (2001), Calculation of peridotite partial melting from thermodynamic models of minerals and melts. IV: Adiabatic decompression and the composition and mean properties of mid-ocean ridge basalts, *J. Petrol.*, *42*, 963–998.

Baker, M. B., and E. M. Stolper (1994), Determining the composition of high-pressure mantle melts using diamond aggregates, *Geochim. Cosmochim. Acta*, *58*, 2811–2827.

Blundy, J., and B. Wood (2003), Partitioning of trace elements between crystals and melts, *Earth Planet. Sci. Lett.*, *210*, 383–397.

Blusztajn, J., N. Shimizu, J. M. Warren, and H. J. B. Dick (2014), In-situ Pb isotopic analysis of sulfides in abyssal peridotites: New insights into heterogeneity and evolution of the oceanic upper mantle, *Geology*, *42*, 159–162.

Bockrath, C., C. Ballhaus, and A. Holzheid (2004), Fractionation of the platinum-group elements during mantle melting, *Science*, *305*, 1951–1953.

Brenan, J. M. (2008), Re-Os fractionation by sulfide melt-silicate melt partitioning: A new spin, *Chem. Geol.*, *248*, 140–165.

Burton, K. W., P. Schiano, J. L. Birck, and C. J. Allegre (1999), Osmium isotope disequilibrium between mantle minerals in a spinel-lherzolite, *Earth Planet. Sci. Lett.*, *172*, 311–322.

Burton, K. W., B. Cenki-Tok, F. Mokadem, J. Harvey, A. Gannoun, O. Alard, and I. J. Parkinson (2012), Unradiogenic lead in Earth's upper mantle, *Nat. Geosci.*, *5*, 570–573.

Crookes, W. (1861), On the existence of a new element, probably of the sulphur group, *Chem. News*, *3*, 193–194.

Donnelly, K. E., S. L. Goldstein, C. H. Langmuir, and M. Spiegelman (2004), Origin of enriched ocean ridge basalts and implications for mantle dynamics, *Earth Planet. Sci. Lett.*, *226*, 347–366.
Falloon, T. J., and D. H. Green (1987), Anhydrous partial melting of morb pyrolite and other peridotite compositions at 10kbar—Implications for the origin of primitive morb glasses, *Mineral. Petrol.*, *37*, 181–219.
Gale, A., C. A. Dalton, C. H. Langmuir, Y. J. Su, and J. G. Schilling (2013), The mean composition of ocean ridge basalts, *Geochem. Geophys. Geosyst.*, *14*, 489–518, doi:10.1029/2012GC004334.
Hart, S. R., and T. Dunn (1993), Experimental cpx melt partitioning of 24 trace-elements, *Contrib. Mineral. Petrol.*, *113*, 1–8.
Harvey, J., C. W. Dale, A. Gannoun, and K. W. Burton (2011), Osmium mass balance in peridotite and the effects of mantle-derived sulphides on basalt petrogenesis, *Geochim. Cosmochim. Acta*, *75*, 5574–5596.
Heinrichs, H., B. Schulz-Dobrick, and K. H. Wedepohl (1980), Terrestrial geochemistry of Cd, Bi, Tl, Pb, Zn and Rb, *Geochim. Cosmochim. Acta*, *44*, 1519–1533.
Hofmann, A. W. (1988), Chemical differentiation of the Earth: The relationship between mantle, continental crust, and oceanic crust, *Earth Planet. Sci. Lett.*, *90*, 297–314.
Hofmann, A. W., and W. M. White (1983), Ba, Rb and Cs in the Earth's mantle, *Z. Naturforsch.*, *38*, 256–266.
Hofmann, A. W., K. P. Jochum, M. Seufert and W. M. White (1986), Nb and Pb in oceanic basalts: New constraints on mantle evolution, *Earth Planet. Sci. Lett.*, *79*, 33–45.
Jenner, F. E., and H. S. C. O'Neill (2012), Analysis of 60 elements in 616 ocean floor basaltic glasses, *Geochem. Geophys. Geosyst.*, *13*, Q02005, doi:10.1029/2011GC004009.
Jochum, K. P., and S. P. Verma (1996), Extreme enrichment of Sb, Tl and other trace elements in altered MORB, *Chem. Geol.*, *130*, 289–299.
Jones, J. H., S. R. Hart, and T. M. Benjamin (1993), Experimental partitioning studies near the Fe-FeS eutectic, with an emphasis on elements important to iron meteorite chronologies (Pb, Ag, Pd, and Tl), *Geochim. Cosmochim. Acta*, *57*, 453–460.
Kelemen, P. B., G. M. Yogodzinski, and D. W. Scholl (2003), Along-strike variation in lavas of the Aleutian Island Arc: Implications for the genesis of high Mg# andesite and the continental crust, *Geophys. Monogr.*, *138*, 223–276.
Kinzler, R. J. (1997), Melting of mantle peridotite at pressures approaching the spinel to garnet transition: Application to mid-ocean ridge basalt petrogenesis, *J. Geophys. Res.*, *102*, 853–874.
Kinzler, R. J., and T. L. Grove (1992), Primary magmas of midocean ridge basalts. 2: Applications, *J. Geophys. Res.*, *97*, 6907–6926.
Kiseeva, E. S., and B. J. Wood (2013), A simple model for chalcophile element partitioning between sulphide and silicate liquids with geochemical applications, *Earth Planet. Sci. Lett.*, *383*, 68–81.
Klein, E. M., and C. H. Langmuir (1987), Global correlations of ocean ridge basalt chemistry with axial depth and crustal thickness, *J. Geophys. Res.*, *92*, 8089–8115.
Lagos, M., C. Ballhaus, C. Munker, C. Wohlgemuth-Ueberwasser, J. Berndt, and D. V. Kuzmin (2008), The Earth's missing lead may not be in the core, *Nature*, *456*, 89–92.
Lamy, A. (1862), De l'existencè d'un nouveau métal, le thallium, *C. R. Hebd. Seances Acad. Sci.*, *54*, 1255–1259.
Lee, C.-T. A., T. C. Lee, and C.-T. Wu (2014), Modeling the compositional evolution of recharging, evacuating, and fractionating (REFC) magma chambers: Implications for differentiation of arc magmas, *Geochim. Cosmochim. Acta*, *143*, 8–22.
Le Roux, V., J. L. Bodinier, A. Tommasi, O. Alard, J. M. Dautria, A. Vauchez, and A. J. V. Riches (2007), The Lherz spinel lherzolite: Refertilized rather than pristine mantle, *Earth Planet. Sci. Lett.*, *259*, 599–612.
Le Roux, V., J. L. Bodinier, O. Alard, S. Y. O'Reilly, and W. L. Griffin (2009), Isotopic decoupling during porous melt flow: A case-study in the Lherz peridotite, *Earth Planet. Sci. Lett.*, *279*, 76–85.
Li, Y., and A. Audetat (2012), Partitioning of V, Mn, Co, Ni, Cu, Zn, As, Mo, Ag, Sn, Sb, W, Au, Pb, and Bi between sulfide phases and hydrous basanite melt at upper mantle conditions, *Earth Planet. Sci. Lett.*, *355*, 327–340.
Liu, Y., N.-T. Samaha, and D. R. Baker (2007), Sulfur concentration at sulfide saturation (SCSS) in magmatic silicate melts, *Geochim. Cosmochim. Acta*, *71*, 1783–1799.
Longhi, J. (2002), Some phase equilibrium systematics of lherzolite melting. I, *Geochem. Geophys. Geosyst.*, *3*(3), 1020, doi:10.1029/2001GC000204.
Lorand, J. P. (1989), Abundance and distribution of Cu-Fe-Ni sulfides, sulfur, copper and platinum-group elements in orogenic-type spinel lherzolite massifs of Ariege (northeastern Pyrenees, France), *Earth Planet. Sci. Lett.*, *93*, 50–64.
Lorand, J. P. (1991), Sulphide petrology and sulphur geochemistry of orogenic lherzolites: A comparative study of the pyrenean bodies (France) and the Lanzo Massif (Italy), *J. Petrol.*, *2*, 77–95.
Lorand, J. P., O. Alard, and A. Luguet (2010), Platinum-group element micronuggets and refertilization process in Lherz orogenic peridotite (northeastern Pyrenees, France), *Earth Planet. Sci. Lett.*, *289*, 298–310.
Luguet, A., J. P. Lorand and M. Seyler (2003), Sulfide petrology and highly siderophile element geochemistry of abyssal peridotites: A coupled study of samples from the Kane Fracture Zone (45 degrees W 23 degrees 20N, MARK Area, Atlantic Ocean), *Geochim. Cosmochim. Acta*, *67*, 1553–1570.
Mavrogenes, J. A., and H. S. C. O'Neill (1999), The relative effects of pressure, temperature and oxygen fugacity on the solubility of sulfide in mafic magmas, *Geochim. Cosmochim. Acta*, *63*, 1173–1180.
McDade, P., J. D. Blundy, and B. J. Wood (2003), Trace element partitioning on the Tinaquillo Lherzolite solidus at 1.5 GPa, *Phys. Earth Planet. Inter.*, *139*, 129–147.
Mckenzie, D., and R. K. Onions (1991), Partial melt distributions from inversion of rare-earth element concentrations, *J. Petrol.*, *32*, 1021–1091.
Melson, W. G., T. O'Hearn, and E. Jarosewich (2002), A data brief on the Smithsonian abyssal volcanic glass data file, *Geochem. Geophys. Geosyst.*, *3*(4), 1023, doi:10.1029/2001GC000249.
Nielsen, S. G., and C. T. A. Lee (2013), Determination of thallium in the USGS glass reference materials BIR-1G, BHVO-2G and BCR-2G and application to quantitative Tl concentrations by LA-ICP-MS, *Geostand. Geoanal. Res.*, *37*, 337–343.
Nielsen, S. G., M. Rehkämper, D. A. H. Teagle, J. C. Alt, D. Butterfield, and A. N. Halliday (2006a), Hydrothermal fluid fluxes calculated from the isotopic mass balance of thallium in the ocean crust, *Earth Planet. Sci. Lett.*, *251*, 120–133.
Nielsen, S. G., M. Rehkämper, M. D. Norman, A. N. Halliday, and D. Harrison (2006b), Thallium isotopic evidence for ferromanganese sediments in the mantle source of Hawaiian basalts, *Nature*, *439*, 314–317.
Nielsen, S. G., M. Rehkämper, A. D. Brandon, M. D. Norman, S. Turner, and S. Y. O'Reilly (2007), Thallium isotopes in Iceland and Azores lavas—Implications for the role of altered crust and mantle geochemistry, *Earth Planet. Sci. Lett.*, *264*, 332–345.
Nielsen, S. G., S. Mar-Gerrison, A. Gannoun, D. LaRowe, V. Klemm, A. N. Halliday, K. W. Burton, and J. R. Hein (2009a), Thallium isotope evidence for a permanent increase in marine organic carbon export in the early Eocene, *Earth Planet. Sci. Lett.*, *278*, 297–307.

Nielsen, S. G., H. M. Williams, W. L. Griffin, S. Y. O'Reilly, N. Pearson, and F. Viljoen (2009b), Thallium isotopes as a potential tracer for the origin of cratonic eclogites, *Geochim. Cosmochim. Acta*, *73*, 7387–7398.
Nielsen, S. G., M. Goff, S. P. Hesselbo, H. C. Jenkyns, D. E. LaRowe, and C. T. A. Lee (2011), Thallium isotopes in early diagenetic pyrite—A paleoredox proxy?, *Geochim. Cosmochim. Acta*, *75*, 6690–6704.
Nielsen, S. G., L. E. Wasylenki, M. Rehkämper, C. L. Peacock, Z. Xue, and E. M. Moon (2013), Towards an understanding of thallium isotope fractionation during adsorption to manganese oxides, *Geochim. Cosmochim. Acta*, *117*, 252–265.
Niu, Y. L. (2004), Bulk-rock major and trace element compositions of abyssal peridotites: Implications for mantle melting, melt extraction and post-melting processes beneath mid-ocean ridges, *J. Petrol.*, *45*, 2423–2458.
Norman, M. D., and M. O. Garcia (1999), Primitive magmas and source characteristics of the Hawaiian plume: Petrology and geochemistry of shield picrites, *Earth Planet. Sci. Lett.*, *168*, 27–44.
O'Neill, H. S. C., and J. A. Mavrogenes (2002), The sulfide capacity and the sulfur content at sulfide saturation of silicate melts at 1400 degrees C and 1 bar, *J. Petrol.*, *43*, 1049–1087.
Prytulak, J., S. G. Nielsen, T. Plank, M. Barker, and T. Elliott (2013), Assessing the utility of thallium and thallium isotopes for tracing subduction zone inputs to the Mariana arc, *Chem. Geol.*, *345*, 139–149.
Rehkämper, M., M. Frank, J. R. Hein, D. Porcelli, A. Halliday, J. Ingri, and V. Liebetrau (2002), Thallium isotope variations in seawater and hydrogenetic, diagenetic, and hydrothermal ferromanganese deposits, *Earth Planet. Sci. Lett.*, *197*, 65–81.
Rehkämper, M., M. Frank, J. R. Hein, and A. Halliday (2004), Cenozoic marine geochemistry of thallium deduced from isotopic studies of ferromanganese crusts and pelagic sediments, *Earth Planet. Sci. Lett.*, *219*, 77–91.
Rubin, K. H., and J. M. Sinton (2008), The ridge filter: How melt supply and magma chambers modulate mantle compositions in MORB, *Geochim. Cosmochim. Acta*, *72*, A810.
Salters, V. J. M., and A. Stracke (2004), Composition of the depleted mantle, *Geochem. Geophys. Geosyst.*, *5*, Q05B07, doi:10.1029/2003GC000597.
Salters, V. J. M., J. E. Longhi, and M. Bizimis (2002), Near mantle solidus trace element partitioning at pressures up to 3.4 GPa, *Geochem. Geophys. Geosyst.*, *3*(7), 1038, doi:10.1029/2001GC000148.
Shannon, R. D. (1976), Revised effective ionic radii and systematic studies of interatomic distances in halides and chalcogenides, *Acta Crystallogr., Sect. A Cryst. Phys. Diffr. Theor. Gen. Crystallogr.*, *32*, 751–767.
Shaw, A. M., M. D. Behn, S. E. Humphris, R. A. Sohn and P. M. Gregg (2010), Deep pooling of low degree melts and volatile fluxes at the 85 degrees E segment of the Gakkel Ridge: Evidence from olivine-hosted melt inclusions and glasses, *Earth Planet. Sci. Lett.*, *289*, 311–322.
Shaw, D. M. (1952), The geochemistry of thallium, *Geochim. Cosmochim. Acta*, *2*, 118–154.
Sobolev, A. V., A. W. Hofmann, S. V. Sobolev and I. K. Nikogosian (2005), An olivine-free mantle source of Hawaiian shield basalts, *Nature*, *434*, 590–597.
Wallace, P., and I. S. E. Carmichael (1992), Sulfur in basaltic magmas, *Geochim. Cosmochim. Acta*, *56*, 1863–1874.
Wanless, V. D., M. R. Perfit, W. I. Ridley, and E. Klein (2010), Dacite petrogenesis on mid-ocean ridges: Evidence for oceanic crustal melting and assimilation, *J. Petrol.*, *51*, 2377–2410.
Warren, J. M., and S. B. Shirey (2012), Lead and osmium isotopic constraints on the oceanic mantle from single abyssal peridotite sulfides, *Earth Planet. Sci. Lett.*, *359*, 279–293.
Wasylenki, L. E., M. B. Baker, A. J. R. Kent, and E. M. Stolper (2003), Near-solidus melting of the shallow upper mantle: Partial melting experiments on depleted peridotite, *J. Petrol.*, *44*, 1163–1191.
Watson, E. B., D. B. Othman, J. M. Luck, and A. W. Hofmann (1987), Partitioning of U, Pb, Cs, Yb, Hf, Re and Os between chromian diopsidic pyroxene and haplobasaltic liquid, *Chem. Geol.*, *62*, 191–208.
Wedepohl, K. H. (1974), *Handbook of Geochemistry*, Springer, New York.
Wood, B. J., S. G. Nielsen, M. Rehkämper, and A. N. Halliday (2008), The effects of core formation on the Pb- and Tl-isotopic composition of the silicate Earth, *Earth Planet. Sci. Lett.*, *269*, 325–335.
Workman, R. K., and S. R. Hart (2005), Major and trace element composition of the depleted MORB mantle (DMM), *Earth Planet. Sci. Lett.*, *231*, 53–72.
York, D., N. M. Evensen, M. L. Martinez, and J. D. Delgado (2004), Unified equations for the slope, intercept, and standard errors of the best straight line, *Am. J. Phys.*, *72*, 367–375.